European Journal of Inorganic Chemistry

EurJIC
European Journal of Inorganic Chemistry

Chemistry Europe
European Chemical Societies Publishing

RESEARCH ARTICLE OPEN ACCESS

Dioxomolybdenum(VI) Complexes Supported by Fluxional Bis(amide)-Functionalized Aminophenolate Ligands

Pasi Vikberg[1,2] | Anssi Peuronen[1] | Manu Lahtinen[3] | Ari Lehtonen[1]

[1]Department of Chemistry, University of Turku, Turku, Finland | [2]Department of Chemistry, University of Helsinki, Helsinki, Finland | [3]Department of Chemistry, University of Jyväskylä, Jyväskylä, Finland

Correspondence: Pasi Vikberg (pasi.vikberg@helsinki.fi) | Ari Lehtonen (arileh@utu.fi)

Received: 27 April 2026 | **Revised:** 10 June 2026 | **Accepted:** 15 June 2026

Keywords: amide | aminophenolate | ligand design | molybdenum | tungsten

ABSTRACT

Benchtop-stable dioxomolybdenum(vi) complexes supported by the new bis(amide) functionalized aminophenolate proligands $\mathbf{H_3L_a}$ and $\mathbf{H_3L_b}$ are reported. Using $[MoO_2(acac)_2]$, $\mathbf{H_3L_a}$ forms the mononuclear complex **Mo1a** in MeOH and the dinuclear, μ-oxo–bridged complex **Mo2a** in aprotic solvents. In contrast, the more sterically hindered ligand $\mathbf{H_3L_b}$ produces the dinuclear complex **Mo2b** regardless of the solvent used. Heavy-oxygen labelling of **Mo2a** with $H_2{}^{18}O$ confirms that water promotes oxo ligand exchange and μ-oxo bridge formation, as evidenced by IR shifts of approximately 50 cm^{-1} to a lower wavenumber for the ν(Mo═^{18}O) and ν(Mo—^{18}O—Mo) stretching vibrations. **Mo1a** has a distorted octahedral Mo centre with an O_3N donor set from $\mathbf{H_2L_a}^-$, two oxides and a methanolate. One of the amide arms remains non-coordinating. **Mo2a** and **Mo2b** have similar coordination spheres, with methanolate replaced by a μ-oxo bridge. **Mo1a** shows hydrolytic instability and poor solubility. Contrarily, the more stable **Mo2a** is fluxional in solution at room temperature (RT) and decomposes above 65 °C. However, low-temperature (–45 °C to –85 °C) ^{1}H NMR reveals distinct signals for the coordinated and non-coordinating amide arms. Tungsten analogues **W1a** (mononuclear) and **W2b** (dinuclear) are isostructural with their molybdenum counterparts. In all complexes, the ligand platform exhibits hemilabile behaviour and solvent-dependent nuclearity.

1 | Introduction

Metalloenzymes are a diverse class of enzymes that carry metal ions in their active sites to accelerate a wide range of biochemical reactions. For example, enzymes containing dioxomolybdenum(vi) and dioxotungsten(vi) centres participate in oxygen atom transfer reactions [1–3], where an oxygen atom is transferred from a donor species to an acceptor molecule [4–6]. Such reactions are essential in biological processes including purine degradation, sulphur metabolism, and detoxification pathways [7]. Model complexes of Mo and W can serve as biomimetic catalysts, replicating the function of natural enzymes such as sulphite oxidase, xanthine oxidase, and aldehyde oxidase. The studies on such model compounds not only advance our understanding of enzyme mechanisms but also contribute to the development of environmentally benign catalytic processes [6]. The catalytic activity of these enzymes is largely attributed to the reactive terminal oxo ligands (M═O), which enable efficient oxygen activation and transfer [8, 9]. Inspired by these natural systems, numerous molecular model complexes have been synthesized to mimic the structure and function of the enzymatic active sites. These models have been extensively investigated for their potential in oxidation catalysis, with applications spanning both academic and industrial domains. Particularly, MoO_2 complexes have demonstrated promising activity in key oxidation reactions such as olefin epoxidation [10, 11], alcohol oxidation [12], deoxygenation [13] of sulfoxides and nitroarenes and deoxydehydration of vicinal diols [13, 14]. These transformations are not only useful in synthetic organic chemistry but also offer routes for biomass conversion and fine chemical production.

MoO_2 complexes with amideamino phenolates (potentially tridentate ONO donor ligands), as well as MoO_2 and WO_2 complexes with amideamino bisphenolates (potentially tetradentate ONO_2 donor ligands), have been studied as active catalysts for alkene epoxidation (Figure 1) [15, 16]. In the dimeric amideamino phenolate complexes, the ligand coordinates to the MoO_2 centre as a monoanionic tridentate ONO donor. This coordination occurs through the phenolate oxygen, the backbone nitrogen of the ligand, and the oxygen atom from the amide group. The octahedral coordination sphere is completed by either a methoxide group or a bridging oxide ion. In the monomeric amideamino bisphenolate complexes, the tetradentate ligand binds to the MoO_2 or WO_2 moiety as an ONOO donor. Coordination involves two phenolate oxygen atoms, the backbone nitrogen, and the oxygen atom from the amide group. In this paper, we report the use of potentially tetradentate diamideamino phenolates to form molecular MoO_2 and WO_2 complexes. Depending on the reaction conditions and proligand used, the complexes either crystallise as a mononuclear species with one methoxy group formed from the deprotonated solvent, or as a dinuclear species with a bridging oxide. The mononuclear species are susceptible to hydrolysis at RT, whereas the dinuclear complexes are much more robust, only decomposing after heating to above 65 °C. The coordinated ligands show considerable fluxionality in the neutral amide groups.

2 | Results and Discussion

2.1 | Syntheses

Proligands $\mathbf{H_3L_a}$ and $\mathbf{H_3L_b}$ were prepared by carbodiimide-mediated peptide coupling of aniline or tert-butylamine with diacid hydrochloride **1·HCl** [17] obtained via **2** [18] (Scheme 1). The peptide coupling reaction conditions were optimized by varying time, bases (TEA = triethylamine, DIPEA = *N*, *N*-diisopropylethylamine), activators (HOSu = *N*-hydroxysuccinimide), and coupling reagents (DCC = *N*, *N*'-dicyclohexylcarbodiimide). For $\mathbf{H_3L_a}$, the highest yield (51%) was obtained using two equivalents each of DCC and aniline in a 5 h, 5 mmol reaction. Yields were not improved upon prolonged reaction times or use of additives such as HOSu, TEA or DIPEA, or excess DCC. In fact, use of any additives caused problems in the reaction workup, lowering the isolated yield in many cases. For example, the addition of three equivalents of DCC relative to **1·HCl** lowered the isolated yield to ca. 27%. Excess DCC complicates workup, and using three equivalents of TEA with two equivalents of HOSu and DCC affords compound **3** bearing an N-phenylimide moiety. $\mathbf{H_3L_b}$ was synthesized analogously, but due to the steric hindrance and lower nucleophilicity of *tert*-butylamine, HOSu was required as an activator; no reaction occurred without it. The proposed mechanisms for the synthesis of proligands as well as **3** are given in Supporting Information (see Schemes **S1**–**S3** and the associated explanations).

All Mo complexes were synthesized in MeOH, $CHCl_3$, or MeCN using equimolar amounts of the proligands $\mathbf{H_3L_a}$ and $\mathbf{H_3L_b}$ and $[MoO_2(acac)_2]$. For the reaction with $\mathbf{H_3L_a}$, the nuclearity of the products depends on the choice of solvent: The mononuclear **Mo1a** is obtained in high yield in MeOH, whereas the synthesis in aprotic solvents such as $CHCl_3$ or MeCN produces a dinuclear μ-oxo-bridged species **Mo2a** in a moderate yield. Notably, however, in reactions involving $\mathbf{H_3L_b}$, the nuclearity of the product is unaffected by the choice of solvent; **Mo2b** is formed even in MeOH. In general, similar solvent-dependent nuclearity has been reported for structurally related MoO_2 complexes [15, 19]. Water was found to be crucial for μ-oxo bridge formation, as **Mo2a-^{18}O**—i.e., the ^{18}O-enriched isotopic analogue of **Mo2a**—forms in the presence of excess ^{18}O-enriched water, as confirmed by IR spectroscopy and ESI-HRMS. A common feature of these complexes is their very limited solubility in usual laboratory solvents aside from DMSO, hampering solution state characterization such as NMR analyses. Furthermore, the monomeric **Mo1a** is hydrolytically unstable upon dissolution in DMSO, with signals corresponding to proligand $\mathbf{H_3L_a}$ visible in the ^{1}H NMR. **Mo2a**, in contrast, remains stable in acetone-d6 or DMSO-d6 at room temperature but undergoes slow decomposition at temperatures above 65 °C. According to ^{1}H NMR spectroscopy, **Mo2a** exhibits significant fluxionality, preventing adequate structural analysis at room temperature (see below).

Related tungsten complexes **W1a** and **W2b** were synthesized for comparison, and detailed synthetic procedures are provided in the Supplementary Material. The reaction of $[WO_2(acac)_2]$ with $\mathbf{H_3L_a}$ in MeOH yielded mononuclear **W1a** as the sole isolable product, whereas $\mathbf{H_3L_b}$ and $[WO_2(acac)_2]$ react to form dinuclear **W2b**. Neither compound is soluble enough in common laboratory solvents, including DMSO, to allow for ^{1}H NMR analysis. However, adequate analysis was possible with ESI-MS in MeCN. The proposed mechanism for the formation of all Mo and W complexes is given in Supporting Information (see Scheme S4 and the accompanying explanation).

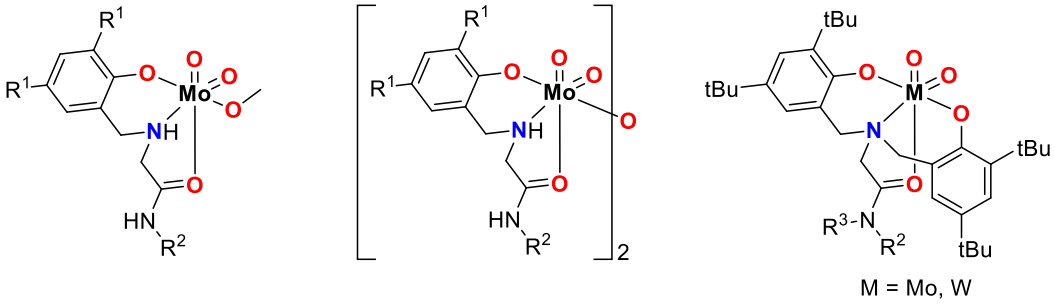

FIGURE 1 | Molybdenum amideamino phenolates and molybdenum and tungsten amideamino bisphenolates. R^1 = tBu, Cl; R^2 = tBu, Ph; R^3 = H, Me [15, 16].

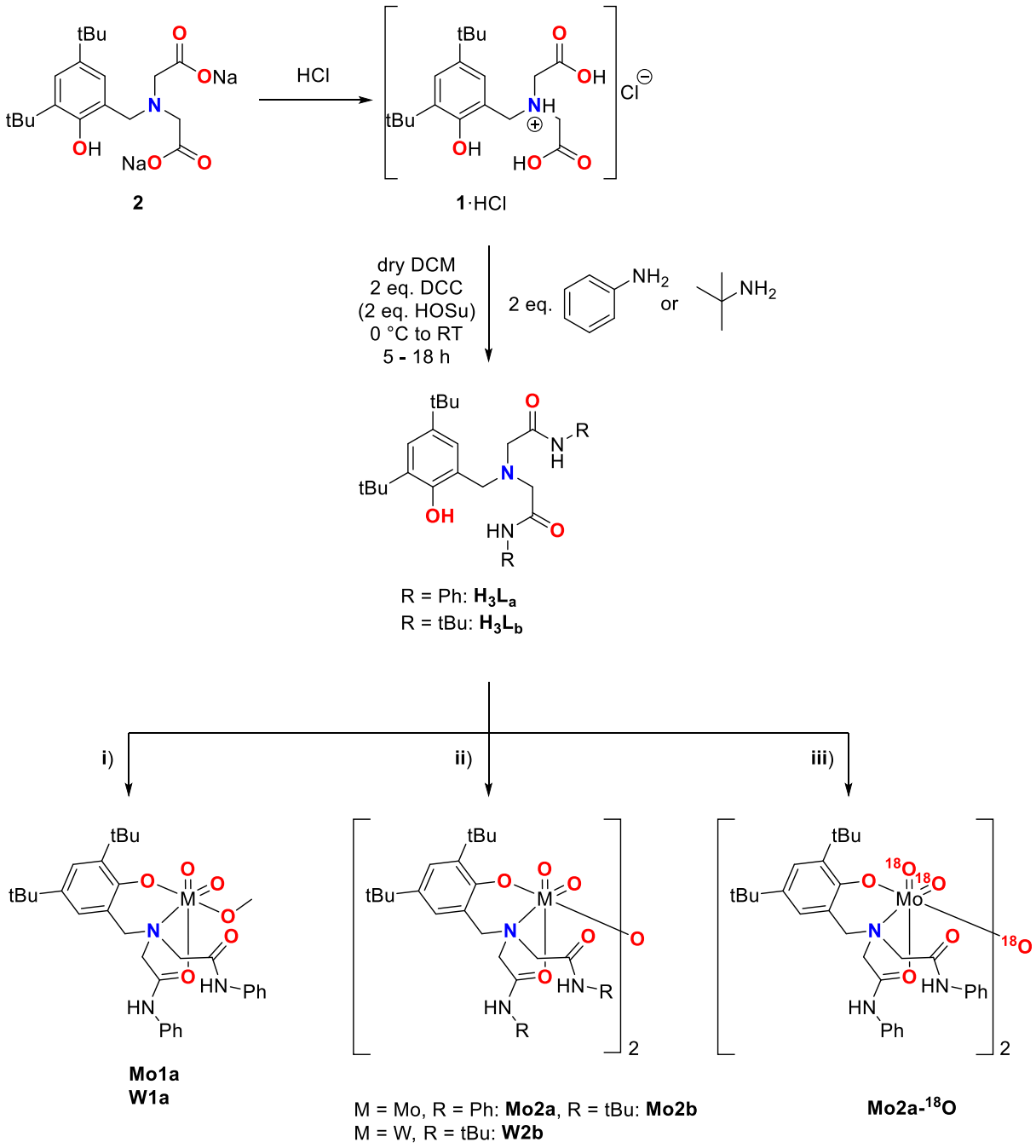

SCHEME 1 | Schematic representation of proligand and complex syntheses. Reaction conditions for the complex syntheses: 1 eq. $\mathbf{H_3L_a}$ or $\mathbf{H_3L_b}$ and 1 eq. $[MO_2(acac)_2]$ (M = Mo, W; $acac^-$ = acetylacetonate) in (i) MeOH, reflux 18 h; (ii) wet MeCN or $CHCl_3$, reflux 18 h; (iii) excess ^{18}O-enriched water, dry $CHCl_3$, reflux 18 h. In the labelling scheme, numbers (1–2) indicate nuclearity, while letters (a–b) identify the aminophenolate ligand.

2.2 | Single-Crystal X-Ray Diffraction

Mo1a, **Mo2a**, and **Mo2b** crystallized readily from their reaction mixtures, and their solid-state structures could be determined by single-crystal X-ray diffraction (SCXRD). The relevant crystallographic data and bond parameters are presented in Supporting Information (Table S2). Mononuclear complex **Mo1a** crystallizes in triclinic space group $P\bar{1}$, whereas the dinuclear complex **Mo2a** crystallizes in monoclinic space group $P2_1/c$ (crystal data of the dinuclear *tert*-butyl acetamide analogue **Mo2b** are presented in Supporting Information). Unlike **Mo1a**, crystals of **Mo2a** emerge as heavily solvated, with four $CDCl_3$ molecules per one **Mo2a** occupying the unit cell. Unfortunately, no crystals suitable for SCXRD could be obtained for **W1a** and **W2b**.

Crystal structure of **Mo1a** consists of two discrete $[MoO_2(\mathbf{H_2L_a})(OMe)]$ molecules in the asymmetric unit (Z = 4). The distorted octahedral coordination environment of the dioxomolybdenum centre in **Mo1a** arises from a O_2N donor set established by the facial coordination of $\mathbf{H_2L_a}^-$ ligand as well as a single methanolate ligand. The $\mathbf{H_2L_a}^-$ ligand is coordinated via one of the two carbonyl groups, central amine and phenolate arm, whereas the second amide pendant arm of the ligand is left uncoordinated (Figure 2). As a result, the complex crystallizes

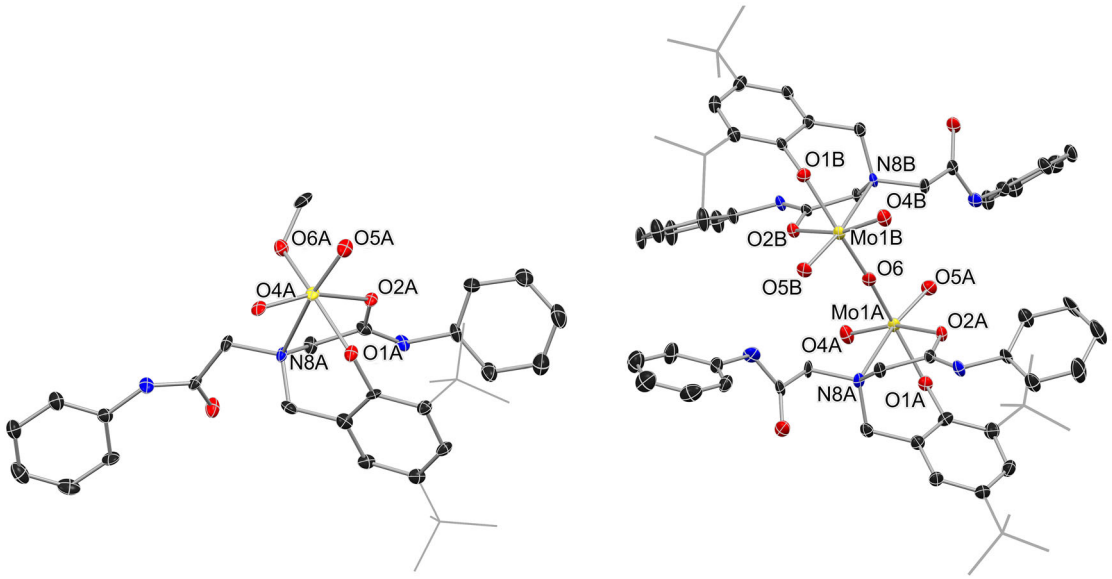

FIGURE 2 | Molecular structures of **Mo1a** (left) and **Mo2a** (right). For **Mo1a**, only one of the two discrete molecular units present in the asymmetric unit is given. C—H hydrogen atoms and solvent molecules are not shown. Displacement ellipsoids are presented at 50% probability level. All H atoms except NH protons have been omitted, and phenol *tert*-butyl groups have been simplified for clarity.

with two chemically identical but crystallographically independent molecules (A and B) in the asymmetric unit. The tridentate coordination of the potentially tetradentate $\mathbf{H_3L_a}$ proligand is a result of the unreached dianionic $\mathbf{HL_a}^{2-}$ charge state of the ligand in the rather mild reaction conditions without the involvement of strong extraneous base. In both discrete complexes the neutral coordinating groups, i.e., amine N and carbonyl O atoms, are each trans to one of the cis MoO_2 oxo atoms, whereas the anionic methanolate and phenolate O atoms are trans to one another. The Mo═O, Mo—N, and Mo—O bond lengths reflect the typical distances of respective Mo—L bonds in the Cambridge Structural Database [20] with the neutral carbonyl Mo—O bond significantly (>0.2 Å) longer compared to the methanolate and phenolate Mo—O— bonds, as expected (Table 1). In typical fashion to amides, the intermolecular packing in the crystal structure is dominated by N—H···O hydrogen bonds, which in the case of **Mo1a** occur to the MoO_2 oxo ions.

TABLE 1 | Selected bonding distances (Å) and angles (°) for Mo1a and Mo2a.

	Mo1a	Mo2a
Distances (Å)		
Mo-O1	1.945(6)/1.971(6)	1.945(4)/1.962(4)
Mo-O2	2.229(6)/2.204(6)	2.225(4)/2.253(4)
Mo-O4	1.716(6)/1.714(6)	1.689(4)/1.705(5)
Mo-O5	1.708(6)/1.718(6)	1.723(4)/1.719(4)
Mo-O6	1.910(6)/1.906(6)	1.901(4)/1.899(4)
Mo-N8	2.478(7)/2.478(6)	2.488(5)/2.449(5)
Angles (°)		
O1-Mo-O6	155.7(2)/153.5(2)	155.78(18)/156.93(18)
O2-Mo-O4	158.3 (2)/155.4(2)	157.39(19)/157.48(19)
O5-Mo-N8	165.7(3)/170.7(3)	167.12(19)/166.70(19)

The solid-state structure of **Mo2a** consists of a μ-oxo bridged dimer in which two ligands cap the dinuclear MoO_2—O—MoO_2 unit (Figure 1). The octahedral coordination environment of each the two Mo centres in the dinuclear complex resemble closely that of **Mo1a** with consistently similar Mo—N and Mo—O distances, including the methanolate and μ-oxo O—Mo distances. Also, the bridging oxo ligand is coordinated trans to the phenolate O atoms in similar fashion to the methanolate in mononuclear complex. The Mo1A–O6–Mo1B angle across the bridging O^{2-} is 174.3(3)°. Despite the lack of crystallographic intramolecular symmetry, the complex is centrosymmetric and thus symmetric NMR spectra can be anticipated. In the crystal structure of **Mo2a** intermolecular hydrogen bonds occur between the N—H donors of the coordinated amide pendant arms and carbonyl acceptors of the uncoordinated, "dangling", amides. Furthermore, the amide N—H atoms of the dangling arms engage in intramolecular hydrogen bonds over the oxo bridge and with the Mo═O oxo atoms of the adjacent molybdenum centre. **Mo2b** has an analogous dimeric structure to **Mo2a** with closely similar bonding parameters around the metal ions (see Figure S35 and Table S1).

2.3 | NMR Spectroscopy

The solution structures of the proligands are unambiguously determined by 1D/2D ^{1}H and ^{13}C NMR spectroscopy. For the complexes, on the other hand, it was only possible to study the solution structure of **Mo2a** due to prohibitively poor solubility of the rest of the complexes. The monomeric variant **Mo1a** either did not dissolve at all (in alcohols) or rapidly hydrolysed in chloroform-d or DMSO-d_6 upon redissolution of its crystals, releasing free ligand $\mathbf{H_3L_a}$. The ^{1}H NMR spectrum of **Mo2a** in acetone-d_6 and DMSO-d_6 at RT is featureless, showing several broad signals with integrals that are not in agreement with respect to the proligand $\mathbf{H_3L_a}$ (see Figures 3 and 4). The severe broadness of the signals led us to speculate that the ligand

backbone of **Mo2a** displays significant fluxionality, hemilability, or both: In principle, the acetanilide pendant arm coordinated to the Mo centre may rapidly oscillate between coordinated and de-coordinated modes. Furthermore, the second and free "dangling" acetanilide pendant arm is free to rotate, move, and possibly coordinate. The way the pendant arms interact with each other may also affect the NMR spectra.

To assess whether fluxionality is the primary cause of signal broadening, variable-temperature ^{1}H NMR investigations were conducted at low and elevated temperatures. For the high-temperature measurements, the ^{1}H NMR spectra of **Mo2a** were recorded in DMSO-d_6 from room temperature (25 °C) to 85 °C in 10 °C increments. The stacked spectra (Figure 3) reveal only minor changes across this range: limited coalescence is observed in signals corresponding to the aromatic rings of the acetanilide pendant arms and the CH_2 bridging groups linking the tertiary amino functionality to the phenol and acetanilide moieties. Notably, thermal decomposition begins at approximately 65 °C, as evidenced by spectra 5–7 in Figure 3, which display additional signals (highlighted by red ellipses) corresponding to the free ligand $\mathbf{H_3L_a}$. This observation underscores the limited thermal stability of **Mo2a** in solution above 65 °C.

Unsatisfied with the results obtained in DMSO-d_6 and at elevated temperatures, low-temperature ^{1}H NMR spectra of a fresh sample of **Mo2a** were recorded in acetone-d_6 at temperatures between +25 °C and −85 °C with an interval of 10 °C (Figure 4). Quite remarkably, all ^{1}H NMR signals of **Mo2a** sharpen to the point that the NMR spectra recorded between −45 °C and −85 °C (Figure 4, spectra 2–6) agree well with the expected structure of the complex and are quite similar to the spectrum of the free ligand $\mathbf{H_3L_a}$ recorded at RT in acetone-d6 in terms of signal sharpness. The most prominent features in the spectra are the divergence of the amide NH, aromatic ArH as well as the *tert*-butyl proton signals. The broad amide signal separates into two well-defined singlets having slightly different chemical shift values of 10.09 and 9.97 ppm, which correspond to the coordinated and dangling acetanilide pendant arms, respectively. Likewise, at RT the signals corresponding to the benzylic CH_2 as well as the CH_2 groups in the acetanilide pendant arms are split into five diastereotopic duplets. Specifically, the acetanilide CH_2 groups are split into two sets of duplets with δ 4.66 and 4.50 ppm, both having a J of ca. 16 Hz, whereas the other set of resonances lie noticeably upfield, at δ 4.22 and 3.83 ppm with a J of ca. 11 Hz. The difference in chemical shift and J-values is another indication of the coordination of only one of the acetanilide pendant arms, as similarly observed in the amide NH shifts. The single benzylic CH_2 group is present at δ 4.39 ppm as a doublet with a J of ca. 5.4 Hz. Collectively, all CH_2 groups are significantly downfield relative to the free ligand $\mathbf{H_3L_a}$, for which the benzylic and acetanilide CH_2 groups appear as singlets at δ 3.92 and 3.57 ppm, respectively.

It was observed that during the measurements at low temperatures, a second minor (∼10%) set of nearly identical ^{1}H NMR resonances started to appear beginning from ca. −15 °C. For example, an additional set of NH amide signals can be observed at δ 10.33 and 9.74 ppm, in addition to the major signals at δ 10.09 and 9.97 ppm, respectively. These signals arise from hindered rotation about the Mo—O—Mo oxo-bridge, especially since the rotation may be expected to slow down to NMR timescale at low temperatures. Another consideration is the potentially labile nature of the coordinated acetanilide pendant arms, which, in principle, is a spectator ligand and may rapidly oscillate between coordinated and de-coordinated modes. At low temperatures, this oscillation may slow down to the point that separate ^{1}H NMR signals for the six-coordinate and pseudo-five-coordinate Mo complexes become visible [15].

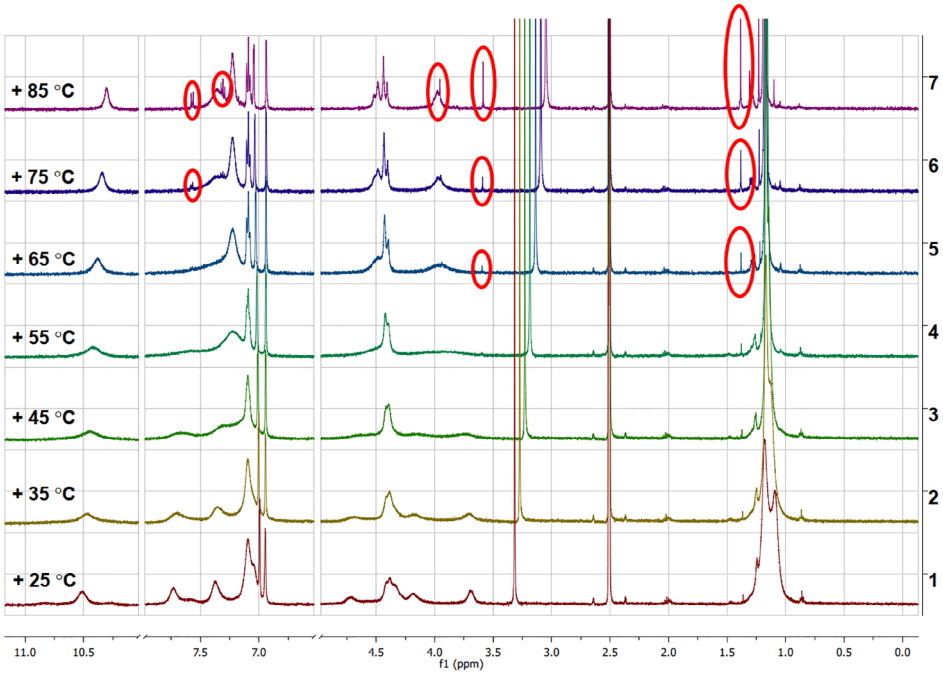

FIGURE 3 | Variable-temperature ^{1}H NMR spectra of **Mo2a** in DMSO-d_6 at temperatures between +25 °C (RT) and +85 °C with 10 °C intervals. At $T \geq 65$ °C, slow decomposition of **Mo2a** begins as illustrated by appearance of signals corresponding to the free ligand $\mathbf{H_3L_a}$ (denoted with red ellipses).

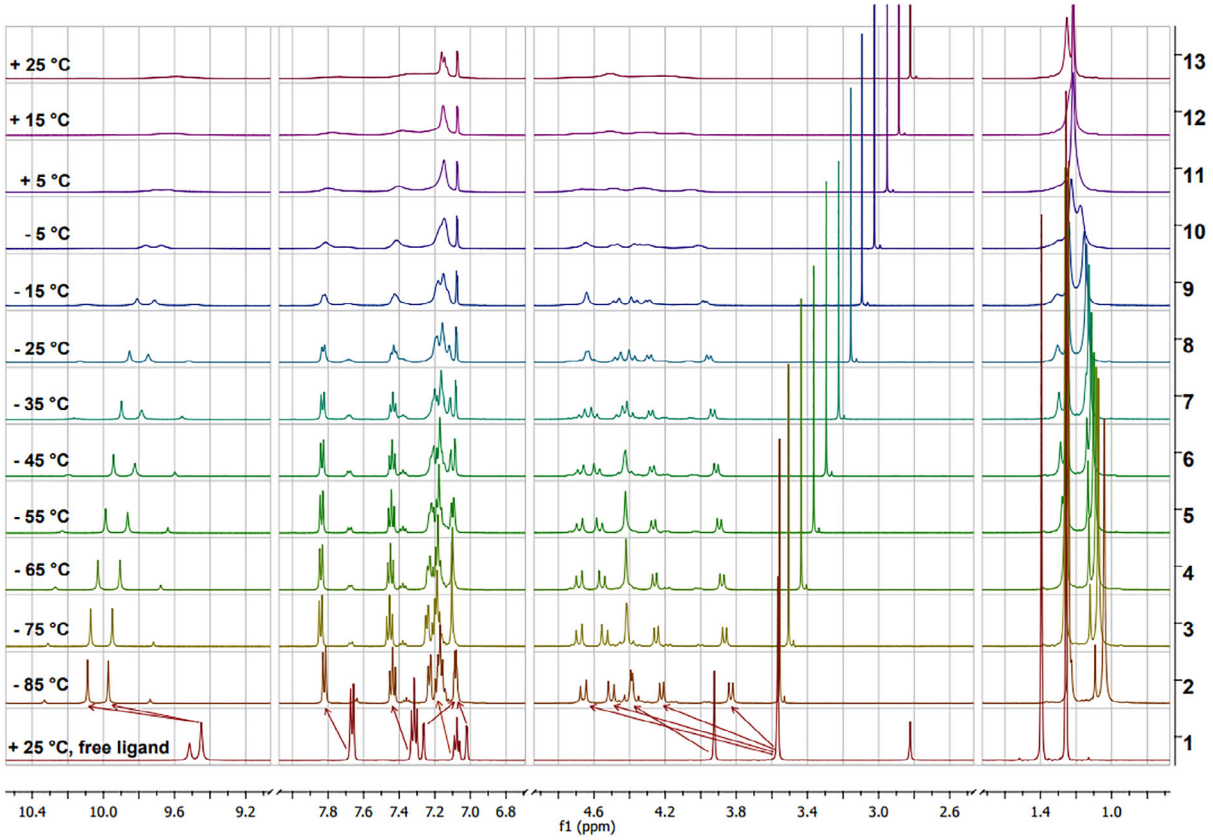

FIGURE 4 | Variable-temperature ^{1}H NMR spectra of **Mo2a** in acetone-d6 at temperatures between + 25 °C (RT) and −85 °C with 10 °C intervals.

2.4 | IR Spectroscopy

All complexes were analysed by IR spectroscopy. The most characteristic features in the IR spectra of **Mo1a**, **Mo2a** and **Mo2b**, as well as those of **W1a** and **W2b** are the stretching vibrations corresponding to the symmetric and asymmetric stretches in the MoO_2 and WO_2 moiety in all complexes, as well as the bridging Mo—O—Mo and W—O—W stretches in the dimeric complexes **Mo2a** and **Mo2a-^{18}O** as well as **W2b** (Table 2). We used ^{18}O-labeling experiments to help determine the assignments of the various MoO_2 IR vibrations. Specifically, all IR signals corresponding to the symmetric and asymmetric MoO_2 as well as Mo—O—Mo vibration modes in **Mo2a-^{18}O** are shifted ca. 50 cm^{-1} in lower frequency in comparison to **Mo2a** [21]. The IR spectra of **Mo2a** superimposed with **Mo2a-^{18}O** are shown in Figure 5. It is observed that the Mo—O—Mo is also shifted to lower frequency in **Mo2a-^{18}O** compared to **Mo2a**, which allowed adequate comparison with other reported dinuclear systems [22–24].

2.5 | Mass Spectrometry

All compounds were analysed by high-resolution mass spectrometry in both in negative and positive modes in MeCN. MS analysis was also possible for the W complexes, which were otherwise too poorly soluble to obtain adequate NMR data. Typically, visible in the positive polarization mode are the sodium adducts of the complexes, whereas in the negative mode, the amide pendant arms are deprotonated to give negatively charged species. Excellent agreement between the experimental masses and isotopic distributions and the corresponding simulated spectra for mono- and dinuclear MoO_2 and WO_2 complexes confirms their formulation, with mass spectrometry proving especially valuable for the characterization of the W complexes. In addition, both positive and negative MS spectra were obtained for the dinuclear **Mo2b-^{18}O** complex, having a mass that is 10 units larger than the non-enriched **Mo2b**. This provides further complementary evidence aside from the IR data suggesting all terminal as well as bridging oxo ligands are exchanged in the presence of heavy

TABLE 2 | Selected IR data for **Mo1a**, **Mo2a**, **Mo2b**, and **Mo2a-^{18}O**, as well as **W1a** and **W2b**.

Compound	$\nu(M=O)_{symm.}$, cm^{-1}	$\nu(M=O)_{asymm.}$, cm^{-1}	$\nu(M–O–M)$, cm^{-1}
Mo1a	905	882	N/A
Mo2a	938	889	737
Mo2a-^{18}O	890	841	697
Mo2b	937	894	741
W1a	929	884	N/A
W2b	943	894	791

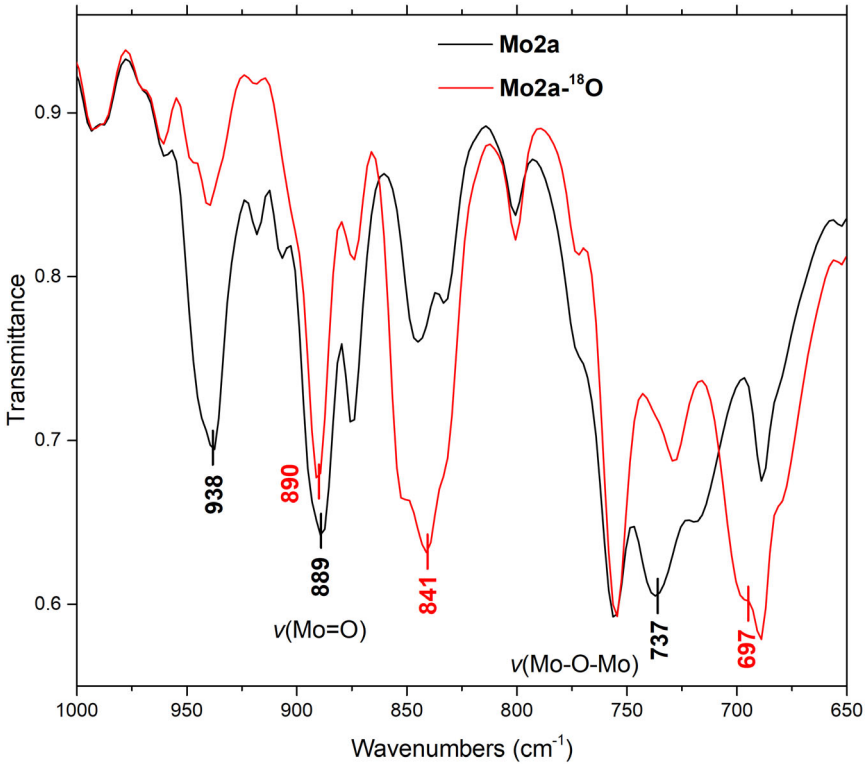

FIGURE 5 | Superimposed IR spectra of **Mo2a** and **Mo2a-^{18}O**, respectively, showcasing the shift in MoO_2 and Mo—O—Mo vibrations.

water. All MS spectra with appropriate analyses are shown in the supplementary material.

3 | Conclusion

In summary and conclusion, this paper describes the synthesis and characterization of benchtop-stable dioxomolybdenum(vi) and -tungsten(vi) complexes based on new bis(amide) functionalized aminophenolate ligands $\mathbf{H_3L_a}$ and $\mathbf{H_3L_b}$. The ligands were designed to integrate a phenol group, tertiary amine nitrogen, and two amide-containing pendant arms to obtain potentially tetradentate, monoanionic ligands. The ligand $\mathbf{H_3L_a}$ reacts with $[MoO_2(acac)_2]$ in methanol to form the mononuclear complex **Mo1a** and in wet aprotic solvents (e.g., MeCN and $CHCl_3$) to form the dinuclear, μ-oxo–bridged complex **Mo2a** due to the presence of water. In contrast, the sterically more hindered ligand $\mathbf{H_3L_b}$ produces the dinuclear complex **Mo2b** regardless of the solvent used. Analogous W complexes **W1a** and **W2b** were synthesized from $[WO_2(acac)_2]$ applying identical synthetic conditions. In solid state, **Mo1a** has a distorted octahedral Mo centre with an O_2N donor set from $\mathbf{H_2L_a}^-$, two oxides and a methanolate. One of the amide arms remains non-coordinating. The coordination sphere of **Mo2a** is comparable to that of **Mo1a**, with the methanolate oxygen being replaced by the μ-oxo bridge. **Mo1a** exhibits hydrolytic instability and poor solubility. In contrast, the more stable **Mo2a** is fluxional in solution at room temperature and decomposes above 65 °C. However, low temperature ^{1}H NMR spectroscopy reveals distinct signals for the coordinated and dangling amide arms. In the future, other functionalities should be investigated, especially ones that offer heightened solubility in common organic solvents. Future applications, also in complexes involving other metals, may see use of the ligands as potentially trianionic and tetra-/hexadentate coordination modes.

4 | Experimental

All syntheses, manipulations, and experiments were done under ambient conditions using analytical-grade commercially available reagents, which were used as received without additional purification or drying procedures, unless stated otherwise. When needed, solvents were dried over activated 3 Å molecular sieves (20% *m/V*) prior to use [25]. $[MoO_2(acac)_2]$ [26] and $[WO_2(acac)_2]$ [27] were prepared according to the published methods. The compound 1·HCl was synthesized via 2 [17] adapting a method by Martell and co-workers [18]. Full description of its synthesis is given in the supporting Information. The IR spectra were measured using a Bruker VERTEX 70 FTIR instrument equipped with a RT-DLaDTGS detector. 64 scans were performed for each individual measurement using a Harrick VideoMVP Single Reflection ATR Microsampler accessory, with a resolution of 4 cm^{-1}. The spectra are measured in transmittance mode, and peaks are reported in wavenumbers (cm^{-1}) and intensities (b = broad, w = weak, m = medium, s = strong, vs = very strong). All NMR spectra were recorded on a Bruker Optics 300 MHz instrument (^{1}H: 300 MHz, ^{13}C: 75 MHz) Bruker Avance III 400 MHz instrument (^{1}H: 400.00 MHz, ^{13}C: 100.59 MHz) or 500 MHz instrument (^{1}H: 500.08 MHz, ^{13}C: 125.75 MHz) equipped with a broad-band smart probes or on a Bruker Avance III 600 MHz instrument (^{1}H: 600.16 MHz, ^{13}C: 150.91 MHz) equipped with a CryoProbe Prodigy triple resonance inverse (TCI) probe, respectively. All ^{1}H and ^{13}C NMR spectra are referenced to

residual solvent signals e.g., $CHCl_3$-H (^{1}H: δ 7.26, ^{13}C: δ 77.16), DMSO-H6 (^{1}H: δ 2.50, ^{13}C: δ 39.52) or to tetramethylsilane (TMS, δ = 0.00 ppm), if present, according to published data [28]. Peaks are reported either as singlets (s), doublets (d), triplets (t), or as combinations thereof, unless the signals are severely broadened, overlapped, or otherwise unresolvable, in which case they are represented as multiplets (m). The coupling constants *J* are given in Hz. ^{13}C NMR spectra were recorded with proton decoupling. High-resolution mass spectra were recorded in MS grade MeCN on a Bruker Daltonics MicroTOF-Q II electrospray ionization time-of-flight (ESI-TOF) mass spectrometer in both positive and negative polarization mode using 5 mM sodium formate solution for calibration. MS results are given as cationic or anionic mass peaks as m/z (mass-to-charge) ratio. Elemental analyses were conducted using a Heraeus Vario CHN Elemental automatic analyzer. Spectroscopic data for all new compounds are presented in the Supporting Information.

4.1 | Single Crystal X-Ray Diffraction

SCXRD data of complexes **Mo1a** [29] and **Mo2a** [29] were collected at 120 K using Rigaku Oxford Diffraction SuperNova instrument equipped with Eos CCD detector using Mo-Kα radiation (λ = 0.71073 Å). Crystallographic data of **Mo2b** [29] were collected using Bruker-Nonius Kappa CCD with APEXII detector (Mo-Kα radiation). CrysAlisPro software was used for data collection and processing of this data [30]. Collection, reduction, and absorption correction of the data were performed using programs COLLECT [31], DENZO and SCALEPACK [32], and SABABS [33]. The structures were solved by direct methods or intrinsic phasing using SHELXS or SHELXT programs [34], respectively. Full-matrix Least Squares refinements on F^2 were performed within the Olex2 program package [35] using SHELXL. All non-hydrogen atoms were refined using anisotropic displacement parameters. Riding atom model was used for all C—H hydrogen atoms, whereas N—H hydrogens were located from the difference density map if possible (weak data quality prohibited this for structure of **Mo1a**). Crystals of **Mo1a** emerged as fibrous needles which were not ideal for SCXRD data collection. Acceptable data were eventually obtained from a crystal showing only minimal signs of additional crystal domains in the diffraction pattern. However, during data reduction, overlapping reflections had to be excluded from the final dataset, resulting in low data completeness.

4.2 | Proligand Syntheses

4.2.1 | H_3L_a

Compound **1·HCl** (1.94 g, 5 mmol) was suspended in 30 mL dry CH_2Cl_2 in a 100 mL round-bottomed flask equipped with a magnetic stir-bar. The suspension was chilled to 0 °C in an ice-water bath, and when cold, treated with *N*, *N*'-dicyclohexylcarbodiimide (2.06 g, 10 mmol). Subsequently, the cooled reaction mixture was stirred for an hour, after which the ice-water bath was removed, and aniline (0.91 mL, 10 mmol) was added. The resulting reaction mixture was stirred for 5 h, then stored in a freezer at −26 °C for an hour to facilitate quantitative precipitation of the *N*, *N*'-dicyclohexylurea by-product and finally vacuum filtered while cold. The CH_2Cl_2 filtrate was evaporated to yield the crude target compound, which was purified by re-crystallization from 40 mL technical MeOH over a period of 3 days. Yield: 1.29 g (51%). ^{1}H NMR (600 MHz, DMSO, 298 K, ppm vs. TMS): δ = 9.97 (s, 2H), 9.73 (s, 1H), 7.58 (dd, *J1* = 7.6 Hz, *J2* = 1.4 Hz, 4H), 7.31 (m, 4H), 7.14 (d, *J* = 2.4 Hz, 1H), 7.05 (tt, *J1* = 7.5 Hz, *J2* = 1.2 Hz, 2H), 6.86 (d, *J* = 2.4 Hz, 1H), 3.89 (s, 2H), 3.61 (s, 4H), 1.37 (s, 9H), 1.19 (s, 9H). ^{13}C NMR (151 MHz, DMSO, 298 K, ppm vs. TMS): δ 169.52, 153.12, 139.79, 138.62, 134.72, 128.81, 124.82, 123.48, 122.66, 122.17, 119.26, 55.92, 55.67, 34.55, 33.71, 31.48, 29.60. IR ATR (cm^{-1}): 3244 m, 3296w, 2960 m, 2901 m, 1676 m, 1596s, 1550vs, 1447s, 1421 m. ESI-MS$^+$: $[M+Na]^+$ ($C_{31}H_{39}N_3O_3Na^+$) calcd. m/z = 524.2884, found m/z = 524.2967. ESI-MS$^-$: $[M-H]^-$ ($C_{31}H_{38}N_3O_3^-$) calcd. m/z = 500.2919, found m/z = 500.2969.

4.2.2 | H_3L_b

Compound **1·HCl** (1.94 g, 5 mmol) and *N*-hydroxysuccinimide (1.15 g, 10 mmol) were suspended in 40 mL dry CH_2Cl_2 in a 100 mL round-bottomed flask equipped with a magnetic stir-bar. The suspension was chilled to 0 °C in an ice-water bath, and when cooled, treated with DCC (2.06 g, 10 mmol). The reaction mixture was then stirred for an hour, after which the ice-water bath was removed, and *tert*-butylamine (1.07 mL, 10 mmol) was added. The resulting reaction mixture was stirred for 18 h at RT, then stored in a freezer at −26 °C for an hour and finally vacuum filtered cold to quantitatively remove *N*, *N*'-dicyclohexylurea by-product. The filtrate was evaporated to yield the crude target compound, which was re-crystallized by dissolution in 20 mL hot technical MeOH, and overnight storage in freezer. Yield: 1.03 g (45%). ^{1}H NMR (500 MHz, DMSO-d_6, 298 K, ppm vs. TMS): δ = 9.73 (s, 1H), 7.54 (s, 2H), 7.14 (d, J = 2.4 Hz), 6.87 (d, J = 2.4 Hz, 1H), 3.61 (s, 2H), 3.06 (s, 4H), 1.38 (s, 9H), 1.24 (s, 19H), 1.23 (s, 9H). ^{13}C NMR (126 MHz, DMSO-d_6, 298 K, ppm vs. TMS): δ 169.91, 152.91, 139.58, 134.70, 125.07, 122.68, 122.33, 56.18, 55.98, 50.14, 34.56, 33.72, 31.51, 29.56, 28.40. IR ATR (cm^{-1}): 3323, 2962 m, 1655, 1550vs, 1480 m, 1361, 1264, 1222s, 938, 881, 648, 578 m. ESI-MS$^+$: $[M+H]^+$ ($C_{27}H_{48}N_3O_3$) calcd. m/z = 462.3690 found m/z = 462.3756. ESI-MS$^-$: $[M-H]^-$ ($C_{27}H_{46}N_3O_3$) calcd. m/z = 460.3545, found m/z = 460.3830.

4.3 | Complex Syntheses

4.3.1 | $MoO_2(H_2L_a)(OMe)$, Mo1a

In a 50 mL round-bottomed flask equipped with a magnetic stir-bar and a reflux condenser was weighed **H_3L_a** (0.200 g, 0.40 mmol) and $[MoO_2(acac)_2]$ (0.130 g, 0.40 mmol). Methanol (30 mL) was added, and the resulting clear, yellow-coloured solution was refluxed ca. 18 h. A yellow microcrystalline solid was subsequently collected by vacuum filtration after the solution had cooled down, washed with small amounts of cold MeOH, and air dried to afford 200 mg **Mo1a** (76%). The filtrate was allowed to slowly evaporate, affording yellow crystals suitable for SCXRD. IR (ATR, cm^{-1}): 3263w, 2951w, 1686w, 1920, 1596, 1442, 1305, 1041 m, 905vs (symm. MoO_2), 882vs (asymm. MoO_2), 846s, 552s, 484 m. ESI-HRMS(+) m/z calcd. for $[M + Na]^+$ $C_{32}H_{41}MoN_3O_6Na$ = 684.1949, m/z found = 684.1929. ESI-HRMS(−) m/z calcd. for $[M - H]^-$ $C_{32}H_{40}MoN_3O_6$ = 660.1984,

m/z found = 660.2040. Anal. Calcd. for $C_{32}H_{41}MoN_3O_6$ (MW = 659.66): C 58.27, H 6.27, N 6.37; found: C 58.17, H 6.04, N 6.33. No NMR data could be obtained due to fast hydrolysis of **Mo1a** upon dissolution in DMSO-d6.

4.3.2 | *{$MoO_2(H_2L_a)$}O, Mo2a*

In a 50 mL round-bottomed flask equipped with a magnetic stir-bar and a reflux condenser was weighed $\mathbf{H_3L_a}$ (0.200 g, 0.40 mmol) and [$MoO_2(acac)_2$] (0.130 g, 0.40 mmol). Chloroform (30 mL) was added, and the resulting bright orange solution was refluxed for ca. 18 h. An orange microcrystalline solid that had formed overnight was collected by vacuum filtration after the solution had cooled down. The solid was washed with 3 × 10 mL $CHCl_3$, and air dried to afford 159 mg **Mo2a** (62%). Orange-coloured crystals suitable for SCXRD could be obtained from a $CDCl_3$ NMR solution upon slow evaporation. **Mo2a** is stable in and well soluble in DMSO and acetone, and slightly soluble in $CHCl_3$ and MeCN, but insoluble in alcohols. ^{1}H NMR (500 MHz, acetone-d6, 188 K, ppm vs. TMS): Major (90%) isomer given only: δ 10.08 (s, 1H, amide NH), 9.97 (s, 1H, amide NH), 7.82 (d, J = 7.7 Hz, 2H, arylamide ArH), 7.44 (t, J = 7.9 Hz, 2H, arylamide ArH), 7.23 (m, 2H, arylamide ArH), 7.17 (m, 4H, arylamide ArH), 7.09 (d, J = 2 Hz, 1H, benzyl ArH), 7.08 (d, J = 2 Hz, 1H, benzyl ArH), 4.66 (d, J = 16 Hz, 1H, benzyl CH_2), 4.50 (d, J = 16 Hz, 1H, benzyl CH_2), 4.39 (d, J = 5.4 Hz, 2H, coordinated acetanilide CH_2), 4.22 (d, J = 11.2 Hz, 1H, non-coordinated acetanilide CH_2), 3.83 (d, J = 11.2 Hz, 1H, non-coordinated acetanilide CH_2), 1.24 (s, 9H, *t*Bu), 1.04 (s, 9H, *t*Bu). IR (ATR, cm^{-1}): 3258w, 1665 m, 1632s, 1599s, 1553s, 1320 m, 1254 m, 938s (symm. MoO_2), 889s (asymm. MoO_2), 755vs, 737vs (Mo—O—Mo), 546vs, 480s. ESI-HRMS(+) m/z calcd. for $[M + Na]^+$ $C_{62}H_{76}Mo_2N_6O_{11}Na$ = 1299.3599, m/z found = 1299.3521. ESI-HRMS(−) m/z calcd. for $[M - H]^-$ $C_{62}H_{75}Mo_2N_6O_{11}$ = 1275.3634, m/z found = 1275.3593. Anal. Calcd. for $C_{62}H_{76}Mo_2N_6O_{11}$ (MW = 1273.24): C 58.49, H 6.02, N 6.60; found: C 58.17, H 5.81, N 6.52.

4.3.3 | *Mo2a-^{18}O*

In an 8 mL air-tight screw-capped scintillation vial was weighed $\mathbf{H_3L_a}$ (32 mg, 64 µmol) and [$MoO_2(acac)_2$] (21 mg, 64 µmol). Three mL dried $CHCl_3$ was added, and the resulting orange reaction mixture was treated with ca. 100 µL ^{18}O-enriched H_2O. The reaction mixture was maintained at 60 °C over a period of 18 h, subsequently cooled at RT and stored in a −26 °C freezer for several days. Afterward, an orange–red microcrystalline solid was isolated by Büchner filtration on a paper filter paper, washed with small amounts of ice-cold $CHCl_3$ and air-dried to yield the target complex with a yield of 23 mg (56%). IR (ATR, cm^{-1}): 3259, 2961w, 1665, 1632, 1599, 1446, 1255 m, 890s (symm. $Mo^{18}O_2$), 841s (asymm. $Mo^{18}O_2$), [21] 755vs, 697vs, 689vs (Mo—^{18}O—Mo), 689vs, 547s, 480s. ESI-HRMS(+) m/z calcd. for $[M + Na]^+$ $C_{62}H_{76}Mo_2N_6NaO_6(^{18}O)_5$ = 1309.3785, m/z found = 1309.3663. ESI-HRMS(−) m/z calcd. for $[M - H]^-$ $C_{62}H_{75}Mo_2N_6O_6(^{18}O)_5$ = 1285.3820, m/z found = 1285.3731.

4.3.4 | *{$MoO_2(H_2L_b)$}O, Mo2b*

Compound $\mathbf{H_3L_b}$ (0.185 g, 0.401 mmol) and [$MoO_2(acac)_2$] (0.130 g, 0.399 mmol) were suspended in 6 mL $CHCl_3$ in an 8 mL air-tight screw-capped scintillation vial and kept at 50 °C for 18 h. Upon standing at RT for several hours, a yellow precipitate was obtained, washed with small amounts of ice-cold $CHCl_3$, and air-dried to yield 126 mg (53%) **Mo2b**. The synthesis was repeated in MeOH, affording the same compound as an orange methanol solvate with a yield of 169 mg (71%). **Mo2b** is stable and insoluble in alcohols, but dissolves well in DMSO and very slightly in MeCN and $CHCl_3$. IR (ATR, cm^{-1}): 3283, 2965, 1658 m, 1624v, 1557, 1476, 1363, 1266, 1219 m, 937s (symm. MoO_2), [21] 894vs (asymm. MoO_2), 850s, 763s, 741vs (Mo—O—Mo), 604 m, 548s. ESI-HRMS(+) m/z calcd. for $[M + Na]^+$ $C_{54}H_{92}Mo_2N_6O_{11}Na$ = 1219.4848, m/z found = 1219.4777. ESI-HRMS(−) m/z calcd. for $[M + Cl]^-$ $C_{54}H_{92}Mo_2N_6O_{11}Cl$ = 1231.4640, m/z found = 1231.4639. The NMR spectra of **Mo2b** at RT are featureless, and unfortunately, no adequate low-temperature NMR spectra could be recorded from **Mo2b** due to its reasonable solubility in DMSO only (mp. = 19 °C).

Acknowledgments

The authors would like to thank the Turku PET Center for the generous donation of ^{18}O-enriched H_2O.

Open access publishing facilitated by Turun yliopisto, as part of the Wiley - FinELib agreement.

Funding

The authors have nothing to report.

Conflicts of Interest

The authors declare no conflicts of interest.

Accession Code

Crystal structure data have been deposited with the Cambridge Crystallographic Data Centre under deposition numbers 2545350 (**Mo2b**), 2545351 (**Mo1a**) and 2545352 (**Mo2a**).

Data Availability Statement

The data that support the findings of this study are openly available in Cambridge Crystallographic Data Centre at https://www.ccdc.cam.ac.uk/, reference number 2545350, 2545351, 2545352.

References

1. C. Andreini, I. Bertini, G. Cavallaro, G. L. Holliday, and J. M. Thornton, "Metal Ions in Biological Catalysis: From Enzyme Databases to General Principles," *Journal of Biological Inorganic Chemistry* 13 (2008): 1205–1218.

2. W. J. Jeong, J. Lee, H. Eom, and W. J. Song, "A Specific Guide for Metalloenzyme Designers: Introduction and Evolution of Metal-Coordination Spheres Embedded in Protein Environments," *Accounts in Chemical Research* 56 (2023): 2416–2425.

3. M. Hoppert, *Encyclopedia of Geobiology*, (Springer, 2011), pp.558–563.

4. J. P. Adamus, A. Ruszczyńska, and A. Wyczałkowska-Tomasik, "Molybdenum's Role as an Essential Element in Enzymes Catabolizing Redox Reactions: A Review," *Biomolecules* 14 (2024): 869.

5. A. Majumdar and S. Sarkar, "Bioinorganic Chemistry of Molybdenum and Tungsten Enzymes: A Structural–functional Modeling Approach," *Coordination Chemistry Reviews* 255 (2011): 1039–1054.

6. S. Pätsch, J. V. Correia, B. J. Elvers, M. Steuer, and C. Schulzke, "Inspired by Nature—Functional Analogues of Molybdenum and Tungsten-Dependent Oxidoreductases," *Molecules* 27 (2022): 3695.

7. R. Hille, C. Schulzke, and M. L. Kirk, "*Molybdenum and Tungsten Enzymes: Biochemistry*," (Royal Society of Chemistry, 2016).

8. K. KC and M. L. Kirk, "*Transition Metals and Sulfur – A Strong Relationship for Life*," M. S. Torres and P. Kroneck (Walter De Gruyter GmbH & Co KG, 2020), pp.313–342.

9. J. Li and U. Ryde, "Comparison of the Active-Site Design of Molybdenum Oxo-Transfer Enzymes by Quantum Mechanical Calculations," *Inorganic Chemistry* 53 (2014): 11913–11924.

10. D. Cvijanović, J. Pisk, G. Pavlović, et al., "Discrete Mononuclear and Dinuclear Compounds Containing a MoO_2^{2+} Core and 4-Aminobenzhydrazone Ligands: Synthesis, Structure and Organic-Solvent-Free Epoxidation Activity," *New Journal of Chemistry* 43 (2019): 1791–1802.

11. S. Mistri and K. Mondal, "Schiff Base-Based Molybdenum Complexes as Green Catalyst in the Epoxidation Reaction: A Minireview," *Topics in Current Chemistry (Z)* 382 (2024): 35.

12. A. Petrov, J. A. Adjei, A. J. Lough, R. S. Wylie, and R. A. Gossage, "Synthesis, Characterization, and Catalytic Exploration of Mononuclear Mo(VI) Dioxido Complexes of (Z)-1-R-2-(4′,4′-Dimethyl-2′-Oxazolin-2′-Yl)-eth-1-en-1-Ates," *Molecules* 27 (2022): 1309.

13. S. Suárez-Pantiga and R. Sanz, "Deoxygenation Reactions in Organic Synthesis Catalyzed by Dioxomolybdenum(vi) Complexes," *Organic & Biomolecular Chemistry* 19 (2021): 10472–10492.

14. J. R. Dethlefsen, D. Lupp, B.-C. Oh, and P. Fristrup, "Molybdenum-Catalyzed Deoxydehydration of Vicinal Diols," *ChemSusChem* 7 (2014): 425–428.

15. N. Zwettler, J. A. Schachner, F. Belaj, and N. C. Mösch-Zanetti, "Hydrogen Bond Donor Functionalized Dioxido-Molybdenum(VI) Complexes as Robust and Highly Efficient Precatalysts for Alkene Epoxidation," *Molecular Catalysis* 443 (2017): 209–219.

16. P. Salonen, J. A. Schachner, A. Peuronen, et al., "Amide Functionalized Aminobisphenolato MoO2 and WO2 Complexes: Synthesis, Characterization, and Alkene Epoxidation Catalysis," *Molecular Catalysis* 540 (2023): 113034.

17. L. Que, R. C. Kolanczyk, and L. S. White, "Functional Models for Catechol 1,2-Dioxygenase. Structure, Reactivity, and Mechanism," *Journal of the American Chemical Society* 109 (1987): 5373–5380.

18. W. R. Harris, R. J. Motekaitis, and A. E. Martell, "New Multidentate Ligands. XVII. Chelating Tendencies of N-(o-Hydroxybenzyl)iminodiacetic Acid (H3L)," *Inorganic Chemistry* 14 (1975): 974–978.

19. M. E. Judmaier, C. Holzer, M. Volpe, and N. C. Mösch-Zanetti, "Molybdenum(VI) Dioxo Complexes Employing Schiff Base Ligands with an Intramolecular Donor for Highly Selective Olefin Epoxidation," *Inorganic Chemistry* 51 (2012): 9956–9966.

20. C. R. Groom, I. J. Bruno, M. P. Lightfoot, and S. C. Ward, "The Cambridge Structural Database," *Acta Crystallographica B* 72 (2016): 171–179.

21. A. Peuronen, R. Sillanpää, and A. Lehtonen, "The Syntheses and Vibrational Spectra of 16O- and 18O-Enriched Cis-MO2 (M=Mo, W) Complexes," *ChemistrySelect* 3 (2018): 3814–3818.

22. W. Wang, T. Guerrero, S. R. Merecias, et al., "Substituent Effects on Solvent-Free Epoxidation Catalyzed by Dioxomolybdenum(VI) Complexes Supported by ONO Schiff Base Ligands," *Inorganica Chimica Acta* 431 (2015): 176–183.

23. W. Wang, J.-C. Daran, R. Poli, and D. Agustin, "OH-Substituted Tridentate ONO Schiff Base Ligands and Related Molybdenum(VI) Complexes for Solvent-Free (ep)oxidation Catalysis with TBHP as Oxidant," *Journal of Molecular Catalysis A: Chemical* 416 (2016): 117–126.

24. A. C. Coelho, M. Nolasco, S. S. Balula, et al., "Chemistry and Catalytic Activity of Molybdenum(VI)-Pyrazolylpyridine Complexes in Olefin Epoxidation. Crystal Structures of Monomeric Dioxo, Dioxo-μ-Oxo, and Oxodiperoxo Derivatives," *Inorganic Chemistry* 50 (2011): 525–538.

25. D. B. G. Williams and M. Lawton, "Drying of Organic Solvents: Quantitative Evaluation of the Efficiency of Several Desiccants," *Journal of Organic Chemistry* 75 (2010): 8351–8354.

26. G. J. J. Chen, J. W. McDonald, and W. E. Newton, "Synthesis of Molybdenum(IV) and Molybdenum(V) Complexes Using Oxo Abstraction by Phosphines. Mechanistic Implications," *Inorganic Chemistry* 15 (1976): 2612–2615.

27. S. B. Yu and R. H. Holm, "Aspects of the Oxygen Atom Transfer Chemistry of Tungsten," *Inorganic Chemistry* 28 (1989): 4385–4391.

28. G. R. Fulmer, A. J. M. Miller, N. H. Sherden, et al., "NMR Chemical Shifts of Trace Impurities: Common Laboratory Solvents, Organics, and Gases in Deuterated Solvents Relevant to the Organometallic Chemist," *Organometallics* 29 (2010): 2176–2179.

29. CCDC deposition numbers: 2545350 (Mo2b), 2545351 (Mo1a), 2545352, Mo2a.

30. Agilent Technologies, (CrysAlis PRO, Agilent Technologies Ltd., 2014).

31. R. W. W. Hooft, *COLLECT* (Nonius BV, 1998).

32. Z. Otwinowski, W. Minor, D. Borek, and M. Cymborowski, *International Tables for Crystallography*, (John Wiley & Sons, Ltd., 2012): 282–295.

33. R. H. Blessing, "Outlier Treatment in Data Merging," *Journal of Applied Crystallography* 30 (1997): 421–426.

34. G. M. Sheldrick, "*SHELXT*– Integrated Space-Group and Crystal-Structure Determination," *Acta Crystallographica Section A Foundations and Advances* 71 (2015): 3–8.

35. O. V. Dolomanov, L. J. Bourhis, R. J. Gildea, J. A. K. Howard, and H. Puschmann, "*OLEX2*: A Complete Structure Solution, Refinement and Analysis Program," *Journal of Applied Crystallography* 42 (2009): 339–341.

36. D. H. Rich and J. Singh, *Major Methods of Peptide Bond Formation*, (Elsevier, 1979), pp.241–261.

Supporting Information

Additional supporting information can be found online in the Supporting Information section. The Electronic Supporting Information associated with this article can be found online. The Supporting Information includes proposed mechanisms for the synthesis of proligands and complex as well as spectral characterizations of all products. The authors have cited an additional reference within the Supporting Information [36].